

NUMERICAL ANALYSIS OF ISOLATED AND INSTALLED SCARFED NOZZLES

By Ardit Ramadani

DEN318 Third Year Project (Aerospace) May 2023

Supervisor: Hussain Ali Abid

SCHOOL OF ENGINEERING AND MATERIALS SCIENCE

ENGINEERING / MATERIALS

THIRD YEAR PROJECT

DEN318

MAY 2023

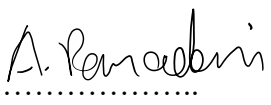
DECLARATION

This report entitled

NUMERICAL ANALYSIS OF ISOLATED AND INSTALLED SCARFED NOZZLES

Was composed by me and is based on my own work. Where the work of the others has been used, it is fully acknowledged in the text and in captions to table illustrations. This report has not been submitted for any other qualification.

Name Ardit Ramadani

Signed 

Date 02/05/2023

The scarfed nozzles SCF001-003 are theorised to reduce the noise of a nozzle in an installed configuration over that of a round cylindrical SMC000 nozzle. The characteristics of these nozzles are analysed in a two-dimensional and three-dimensional RANS model in an isolated and installed configuration, modelling a flat semi-infinite plate as a nearby surface such as a wing. The parameters of the theoretical setup are modelled on the experimental study on scarfed nozzles from the University of Bristol, including the nozzle diameter and installation characteristics. The three-dimensional model was validated against experimental data, the jet deflection on the XY plane was observed and quantified at several downstream spanwise distances, as well as the turbulent kinetic energy. Jet-plate interaction was monitored along the surface of the plate through near field Proudman acoustic power to conclude the reduction of interaction with the angle of scarfing on the nozzle.

Table of Contents

1	Introduction	7
1.1	Motivation	7
1.2	Background and Theory	8
1.3	Aims	8
1.4	Objectives.....	9
2	Literature Review	9
2.1	Jet Installation Noise	9
2.2	Scarfed Nozzle experimental studies	10
2.3	Computational Noise Prediction Tools	11
3	Methodology.....	13
3.1	Geometry.....	13
3.2	Mesh.....	14
3.3	Boundary Conditions.....	17
3.4	Data Collection.....	18
3.5	Solvers and Models	19
4	Results	20
4.1	Mesh Independence Study	20
4.2	Preliminary Validation	22
4.3	Result Convergence.....	23
4.4	Experimental Validation	24
4.5	Scarfed Nozzle Jet Deflection.....	25
4.6	Turbulent Kinetic Energy.....	29

4.7	Acoustics	31
4.8	Computational Expenses	33
5	Conclusion	33
6	References	35
7	Appendix	36
7.1	Velocity scalar scenes for section 4.5	37
7.2	Turbulent kinetic energy scalar scenes for section 4.6.....	38

List of Figures

•	Figure 1: Nozzle classification [7]	13
•	Figure 2: Installed Plate setup [7]	14
•	Figure 3: Z-axis cross section of a) SMC000 mesh, b) SCF004 mesh	15
•	Figure 4: Installed SMC000 mesh	15
•	Figure 5: Close up visualization of mesh for SCM000.....	16
•	Figure 6: Boundary layer for SMC000	17
•	Figure 7: SMC000 boundary conditions.....	18
•	Figure 8: Installed SMC000 boundary conditions	18
•	Figure 9: PlateLine, LipLine and CentreLine probes	19
•	Figure 10: Downstream probes	19
•	Figure 11: a) 2D, b) 3D mesh independence	21
•	Figure 12: Wall Y+ distribution on a) external and b) internal nozzle surface	22
•	Figure 13: RANS vs LES velocity variation with axial distance [8].....	22
•	Figure 14: a) 2D Lip and Centre Line plots, b) 3D Lip and Centre line plots installed vs isolated.....	23
•	Figure 15: Sample Residual and velocity magnitude plots showing convergence.....	23
•	Figure 16: Experimental vs Numerical data for SMC000 nozzle.....	24
•	Figure 17: Two-Dimensional SMC000 standardized velocity with radial distance for $x/D_j = 1,3,5,7,10,15$	25
•	Figure 18: SMC000 and SCF004 jet plume deflection in installed and isolated scenarios	25
•	Figure 19: Radial standardized velocity variation for $x/D_j = 1,3,5,7,10,15$ (Isolated)	27
•	Figure 20: Radial standardized velocity variation for $x/D_j = 1,3,5,7,10,15$ (Installed).....	28
•	Figure 21: Turbulent Kinetic Energy on XY plane for SMC000 and SCF004 nozzles in isolated and installed scenarios	29
•	Figure 22: Tke variation in the radial direction at $x/D_j = 3,5,7,10,15$ for all nozzles in isolated vs installed scenarios	30
•	Figure 23: Proudman Acoustic Power for all installed nozzles on XY plane	31
•	Figure 24: Proudman acoustic power along the lower plate surface for installed nozzles	32
•	Figure 25: Installed and Isolated velocity scalar scenes for nozzles SCF001-003	37
•	Figure 26: Installed and Isolated turbulent kinetic energy scalar scenes for nozzles SCF001-003	38

List of Tables

Table 1: Boundary layer thickness calculation values	16
Table 2: Prism layer values	17
Table 3: 2D mesh independence values. Chosen value highlighted	20
Table 4: 3D mesh independence values. Chosen value highlighted	21
Table 5: Peak to peak difference	24
Table 6: Jet deflection angles	26
Table 7: Plate interaction reduction for installed scarfed nozzles	33

List of Symbols

D_j	Jet exit diameter
H	Radial plate distance from origin
L	Downstream plate length
T_s	Stagnation temperature
T_j	Jet temperature
Y^+	Dimensionless distance from wall
Re	Reynolds number
V	Velocity
d	Diameter
x	Axial distance
U	Spanwise velocity
U_j	Jet exit velocity
r	Radial distance
μ	Dynamic viscosity
ρ	Density
ε	Turbulent dissipation rate

List of Abbreviations

ICAO	International Civil Aviation Organisation
EPNdb	Estimated Perceived Noise (dB)
Tke	Turbulent kinetic energy
SPL	Sound Pressure Level
RANS	Reynolds-Averaged Navier-Stokes
BJARF	Bristol Jet Aeroacoustics Research Facility
LES	Large Eddy Simulation
WMLES	Wall Modelled Large Eddy Simulation
FW-H	Ffowcs Williams-Hawkings
hrt	Hour Run Time

1 Introduction

1.1 Motivation

The International Civil Aviation Organization is the governing body in charge of setting out restrictions and guidelines for the future development of the aviation industry. The ICAO regulations have evolved over the years to match the problems which arise from such rapid development in the field of aviation. Many annexes have been added to the ICAO guidelines, one of such being Annex 16, tasked with environmental protection and the reduction of many forms of pollution, including that of noise pollution [1]. While noise pollution may not be a big factor in sparsely populated areas, the millions of people which live in close proximity to an airfield or directly under a commercial flight path suffer greatly in their everyday lives. Annex 16 has set out a roadmap entailing the gradual reduction in Effective Perceived Noise (EPNdB) in Decibels per Maximum Take-off Mass of an aircraft, with a reduction of 14-24 dB by 2028 [2], depending on aircraft type. Achieving Aircraft Noise Certification is crucial for the operation of an airline which forces manufacturers to constantly develop and implement new measures for the total noise reduction of their aircraft.

With the growing demand for commercial air travel, airlines are requiring the manufacture of larger aircraft in order to improve logistics and keep the cost per passenger low for a flight. This directly conflicts with the ICAOs guidelines as it calls for more powerful engines which ultimately produce more noise. In addition to this, manufactures are constantly increasing the bypass ratio of their engines to increase the efficiency of their aircraft and due to ground clearance requirements, the engines are having to be mounted in closer proximity to other airframe surfaces further amplifying their noise [3]. The ICAO analysis of the sources of noise pollution in twin aisle aircraft within Annex 16 [1] gives a breakdown of their relative significance, it conveys that the largest source of noise pollution is that of the engine during take-off, which is further compartmentalised into five subcategories of which Jet noise is the second largest contributor after fan noise. This is due to the excess thrust required to accelerate the aircraft and operate the high lift devices during take-off, which coincidentally is the flight condition where noise pollution is most disruptive. With Jet noise being such a significant contributor in the total EPNdB of an aircraft, even a small percentage decrease in jet noise could lead to a dramatic reduction in the aircrafts overall noise output.

This has created a huge demand for jet noise reduction devices and while manufacturers are already implementing features to reduce the noise of the isolated engine itself, there is a lot of potential noise performance benefits to be had from the reduction of jet installation noise.

1.2 Background and Theory

Modern commercial aircraft operate in the subsonic region and use high bypass turbofan engines to provide thrust. These engines use several compression and combustion processes in order to accelerate gasses through the core to produce the majority of their thrust as well as bypassing air around the core in order to increase efficiency. The combustion gasses eventually flow to the exhaust where they pass through a convergent exhaust nozzle designed to further accelerate these gasses and increase the total thrust power of the engine [4]. Many nozzle optimisations have been attempted in order to reduce the jet noise, one of such being the SMC006 chevron nozzle, which increases the jet mixing to reduce noise propagation even in an isolated scenario [5]. Another form of noise reduction design in nozzle geometry is that of the scarfed nozzles, namely SCF001 – SCF004, which induce asymmetry in the jet flow and deflect flow away from an airframe surface in order to reduce noise in an installed scenario.

It has been shown by Brown that the installation noise is proportional to the distance between the adjacent surface and centreline of the jet [3] meaning that the jet noise is further amplified by this “scrubbing” and “scattering” phenomenon occurring on the plate surface and trailing edge respectively. This suggests that the successful deflection of an engines jet away from the target surface as attempted by the SCF nozzles would therefore theoretically reduce the installation noise of the engine when mounted near a surface.

1.3 Aims

This paper aims to develop a computationally resource efficient numerical analysis of the scarfed nozzles SCF001-004 in an isolated and installed configuration using the Reynolds Averaged Navier-Stokes equations in order to assist further development of nozzle geometries. This would lead to an overall reduction in EPNdB which is crucial for achieving aircraft noise certification from the ICAO as well as improving the quality of life for people living around busy airfields.

1.4 Objectives

- Produce a two and three-dimensional RANS model for the SMC000 and SCF001-003 nozzles
- Simulate a Mach flow number of 0.5
- Monitor the deflection angle for the different nozzles
- Validation against experimental data
- Velocity magnitude and turbulent kinetic energy analysis
- Produce a far field noise model

2 Literature Review

2.1 Jet Installation Noise

Many studies have been conducted into jet surface interaction and the effects it has on the sound pressure level (SPL) and far field acoustics in an installed configuration as compared to a jet in an isolated configuration, including that of Mead [6] and more recently, and notably, Brown [3]. Mead investigated the jet installation noise through various scenarios ranging from the typical flat plate in a stationary configuration, as is common in most jet installation noise research, to an installation on a “realistic wing geometry” under simulated flight conditions. Mead was able to conclude an increase of approximately 2 dB at high and 9 dB at low noise frequencies and, that there were no major changes to the reflected jet noise under simulated flight conditions. The experiment by Mead also showed that while the Sound Pressure Level results were not consistent between the flat plate and realistic wing geometry conditions, the general trend in the changes in sound pressure level between tests with their respective geometries was consistent, and that the use of a flat plate to model an airframe surface can prove simple yet effective.

Brown further develops the research into installed jet noise and the Jet surface interaction by introducing a new set of test parameters including the plate in a shielding as well as reflecting scenario and incorporating various heated and unheated subsonic and supersonic jets [3]. The report set out to quantify a large data set on which future investigation can be compared and validated against. The investigation was carried out in the NASA Glenn Research Facility within the Aero Acoustics Propulsion Lab which is a highly validated facility capable of producing accurate and reliable readings making it a suitable basis for validation of future work. The test scenarios used a round convergent nozzle to test subsonic flows in an isolated

case as well as installed scenarios for a range of downstream plate lengths (L), varying from 2 to 20 nozzle diameter lengths (D_j), and horizontal plate distances (H), varying from 1 to 16 nozzle diameter lengths. The subsonic experimental tests relative to this report were conducted at a temperature ratio of $T_s/T_j = 0.95$ and Mach number of 0.5, at horizontal plate – jet distances (H) of 1,2,3,5,10 D_j .

Mead and Brown have supplied a high-quality data set among which further investigation can be validated. The limitations of these reports lie in their limited use of the round SMC000 type nozzle which does not possess any specific noise reduction properties however as stated by Brown [3], the results were supplied with the intention of determining regions where more testing is required and enabling the development of future aircraft noise prediction tools. The SMC000 data allows for a basis for the RANS analysis data to be validated against in order to then transition to the SCF scarfed nozzle models.

2.2 Scarfed Nozzle experimental studies

An experimental study has been conducted into the use of Scarfed Nozzles for jet installation noise reduction by Kamliya Jawahar, H. & Azarpeyvand, M [7] at the University of Bristol. The study was conducted in the Bristol Jet Aeroacoustics Research Facility (BJARF) which is capable of producing a clean quiet jet for various jet exit Mach numbers and, the BJARF has been thoroughly validated through other studies and can be considered a reliable source of experimental validation for computational noise prediction models. The study investigated the scarfed SCF001 – 004 nozzles as compared to the round symmetrical SMC000 nozzle through a jet exit Mach number of 0.5 and 0.7 and the effect the scarfing angle had on sound pressure levels, assuming a constant jet exit diameter. Characteristics of the jet hydrodynamic pressure were also studied in the far field axial direction with nearfield measurements being taken via surface pressure transducers on the installed plate. Spectral, coherence and correlation analysis were carried out to determine the noise reduction mechanisms at the proximity of the flat plate.

Far field measurements were taken using microphones in a polar array centred around the nozzle exit, from 50 degrees upstream to 150 degrees in the downstream direction. There are slight discrepancies throughout the report in the classification of the experimental set up with, the microphone array being listed as both 40 and 42 jet diameters away, and the plate being labelled as 7 diameters in length however it only spanning 4 diameters downstream and 2 diameters up stream of the nozzle exit. Regardless of this, the report can still be assumed to be

accurate and reliable as the facility is well regarded and validated against other reports, while following the trends established by Brown [3]. The correct experimental set up is assumed to be; an unheated subsonic jet, far field measurements at a distance of 42 jet diameters radially from the nozzle exit, a plate length of 6 jet diameters, two of which being up stream and 4 being downstream of the nozzle exit, a horizontal plate – jet centreline distance of 1 jet diameter, and a jet exit diameter of 38.1mm.

Jawahar & Azarpeyvand found that in the far field, noise measurements did not show any difference between the round and scarfed nozzles for most polar angles. Scarfed nozzles in isolated configurations showed a marginal increase in the low frequency region and a considerable reduction in the high frequency region, and in an installed configuration showed considerable reduction in the low frequency region and substantial increase in the high frequency region. The report concluded that more research is required to understand the flow field and noise reduction characteristics of scarfed nozzles and provided a large data set among which results from this report can be compared and validated against.

2.3 Computational Noise Prediction Tools

Lyu, B et al [8] used a low order RANS model to predict the installed jet noise of a symmetrical round convergent nozzle. The report used two noise contribution sources via different analytical methods, using a half plane scattering greens function for the near field evanescent wave scattering and sound induced by the turbulent Lighthill's quadrupole sources in the far field. This proved to provide quantitative agreement to experimental data for the 90-degree polar angle, however this could not be achieved universally as this method neglected the jet refraction effect which is significant at low observer angles and high frequency regions. The report also investigated the same conditions using the unsteady LES, which is a far more computationally expensive model, however, was able to achieve more coherent results. Lyu, B et al showed that while the RANS modelling of an installed jet is not as accurate as the LES, it can still be an effective way to get a preliminary understanding of the problem as an LES simulation can take several days to weeks to turn around. RANS modelling also provided validated data at the 90-degree reflected angle which could be considered to be the most significant polar angle as it would have the shortest path to the observer on the ground and therefore the least dissipation.

Another significant study to have arisen in the aero acoustics field from the University of Bristol BJARF is the study of the effects of chevrons on jet installation noise by Jawahar H et al [5]. This is a predecessor to the scarfed nozzle study also by Jawahar H, and investigates the use of chevron nozzles for the reduction of installed jet noise via experimental and numerical methodologies. Chevron nozzles are already known to decrease jet noise at low frequencies in an isolated configuration and Jawahar H et al investigated experimentally the effects of installed noise at several different plate distances, Mach numbers and chevron nozzle types, SMC000-006. The jet hydrodynamic pressure fluctuations were measured in the far field axial direction on the reflected side and the data compiled is a quantitative and reliable basis upon which a numerical method can be developed. The study then went on to build a numerical model of the SMC000, which is significant to this report, and the SMC006 chevron nozzle using the LES flow model together with the Ffowcs Williams-Hawkings (FW-H) equation to predict the far field sound pressure levels. The report concluded that the LES FW-H models established were validated against the experimental data with a 1-2dB agreement in the far field and that the modelling of the round jet agrees with previous literature. This further supports that accurate models can be produced using LES however as with previously mentioned literature, the LES model is computationally expensive and RANS models are not widely incorporated, leading to a gap in effective yet computationally inexpensive models.

One attempt to model an installed convergent nozzle in a more computationally effective method is that by Abid H et al [9] where Wall Modelled LES (WMLES) are used to produce the basis for the FW-H method. The LES method uses a prism layer type mesher which refines the grid size significantly in the normal direction close to a surface, which results in a substantially larger number of grid points, in order to capture the flow interaction with a no slip wall using a low Y^+ [10]. The WMLES uses wall modelling functions to account for the flow close to the surface meaning a large Y^+ can be used and the mesh refinement close to the surface is not required. The WMLES still uses the LES turbulence model for freestream flow meaning that while more efficient than traditional LES, WMLES is still a computationally intensive model. The report in question investigated the SMC000 and SMC006 nozzles using the WMLES and was able to achieve a robust jet installation prediction tool. The report however incorporated the use of high-performance GPUs to accelerate the LES computation which are unavailable for this investigation. The findings of [9] outline the areas where plate interaction and noise sources are most substantial, allowing the scarfed nozzle analysis to be carried out to focus on these areas of interest.

2.4 Summary

Extensive experimental research has been conducted on the installed and isolated characteristics of the round symmetrical nozzle [3], [5]–[7], allowing for future work to be effectively validated for several operating conditions. Many well validated and robust noise prediction models have been achieved for the SMC nozzles using predominantly WMLES and LES [5], [8], [9], with some less extensive RANS models existing [8]. The experimental and numerical models have outlined areas of importance when attempting an installed nozzle model, those being; the boundary layer interaction in the nozzle, surface interaction along the plate, scattering on the plate trailing edge and the radial distance between the nozzle centreline and plate. The review has shown that while many robust analysis models exist, the computational requirements and turnaround for these models is substantial, they are limited to the symmetrical SMC000-006 nozzles and that the need for an efficient model as well as analysis for the scarfed nozzles exists.

3 Methodology

3.1 Geometry

The jet configurations and flow conditions are taken from Jawahar H et al [7] and modified using Autodesk Inventor in order to have a consistent jet exit diameter across all nozzles, with the nozzles in the scope of the investigation being the round cylindrical nozzle SMC000 and scarfed nozzles SCF001, SCF002, SCF003 and SCF004 as represented in Figure 1.

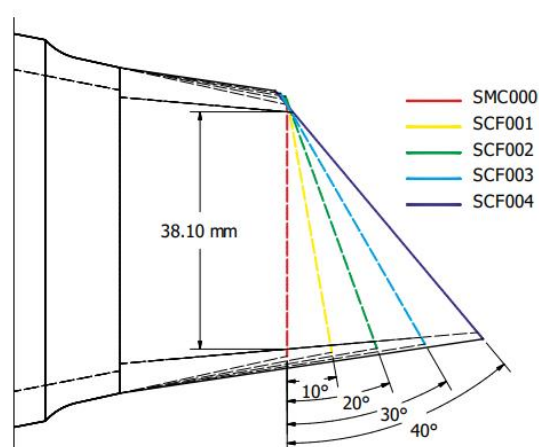


Figure 1: Nozzle classification [7]

The jet exit diameter is 38.1mm with a scarf angle between 10° to 40° . For the installed configuration a semi-infinite plate of length $6D_j$ is placed at a horizontal distance $1D_j$ away from the jet centreline and spans a distance $4D_j$ downstream and $2D_j$ up stream of the jet exit as represented in Figure 2. The plate is 5mm thick and chamfered at 30° creating a sharp edge on the trailing edge of the plate, all other edges are flat. A cross section of the 3-dimensional nozzles was taken using Autodesk Inventor in order to form the volume for the 2-dimensional test case.

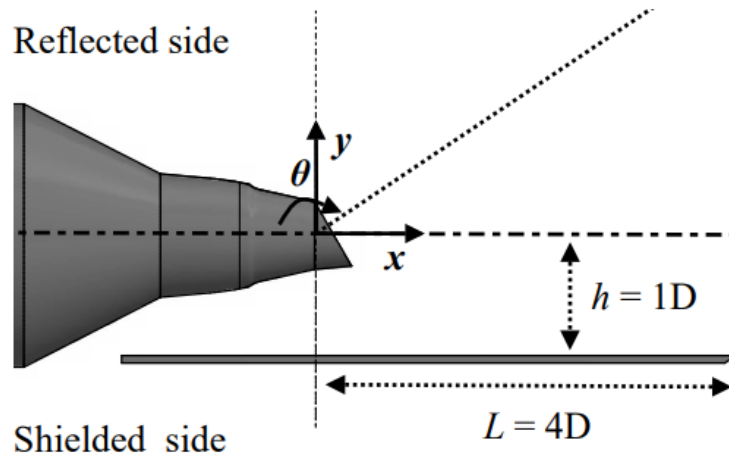


Figure 2: Installed Plate setup [7]

3.2 Mesh

A cylindrical control volume was used to encapsulate the nozzle and jet flow, with a cylinder radius of $10D_j$ and length $40D_j$ downstream of the nozzle origin. A non-uniform Trimmed Cell Mesher was used for all test scenarios with a two-axis symmetric mesh for the SMC000 nozzle and a Z-axis symmetrical mesh for the SCF001-004 nozzles, generated within STARCCM+. The mesh consisted of several regions of varying mesh density with high density areas within the nozzle contraction, along the plate and upper and lower lip lines, and lower density far outside and downstream of the jet. The mesh consisted of a total cell number of 2.578 million, and the independent mesh density areas were generated using various cone geometries within STARCCM+.

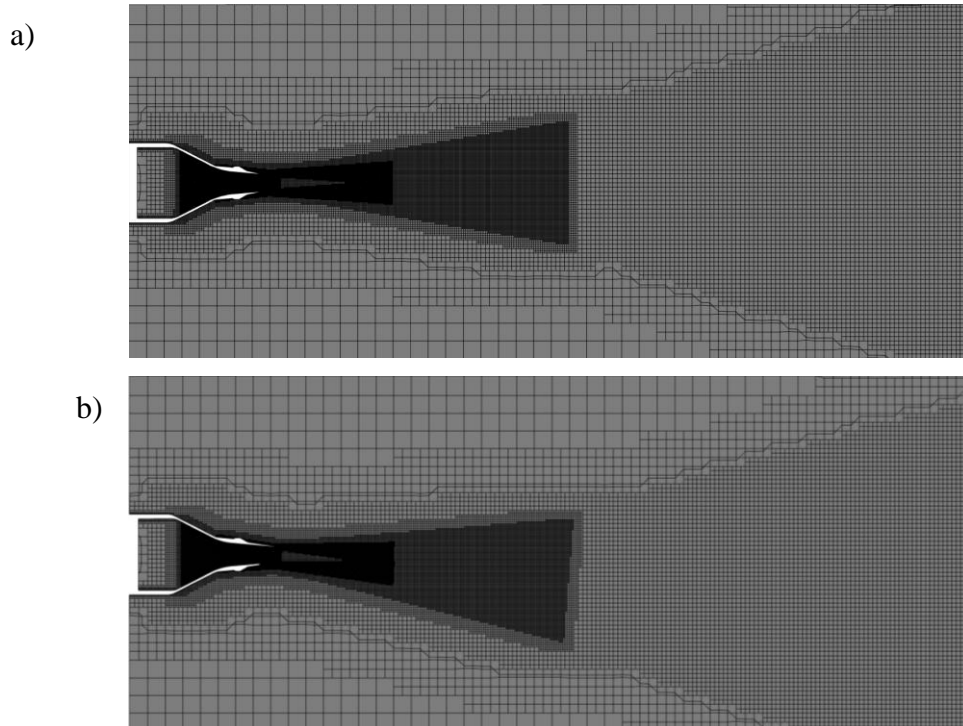


Figure 3: Z-axis cross section of a) SMC000 mesh, b) SCF004 mesh

The cone refinement regions are designed to coincide with areas of large velocity gradients, the mesh is most refined in the nozzle contraction where the flow is accelerated and experiences the largest gradient, this is followed by a refinement at the upper and lower lip lines of the nozzle to encapsulate the gradient due to dissipation of the jet core, as shown in Figure 3. The cone mesh geometries for the SMC000 nozzle span solely in the horizontal direction whereas the scarfed nozzle mesh geometries are angled in the negative Y direction in order to follow the deflected jet core. For installed test cases an additional rectangular region of refinement is implemented around the plate to account for any jet plume-plate interaction that may occur.

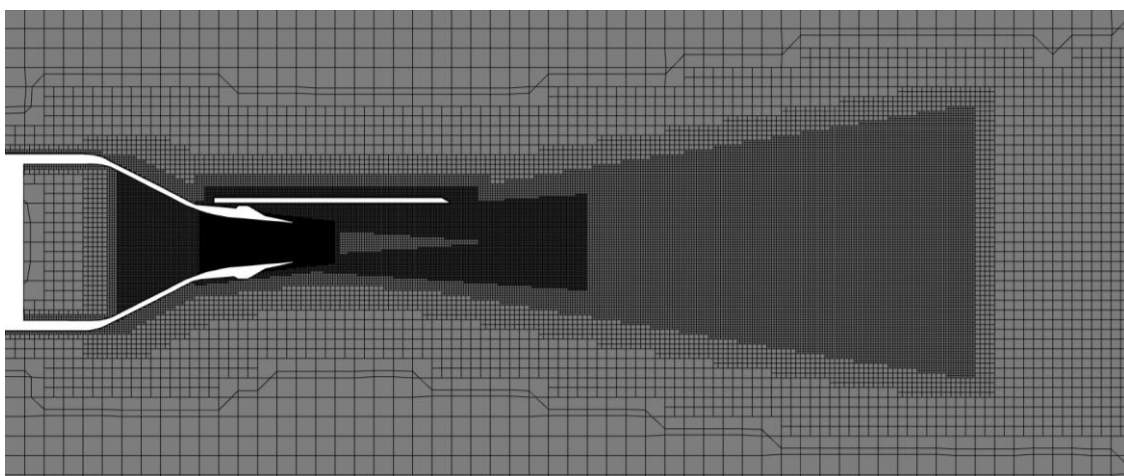


Figure 4: Installed SMC000 mesh

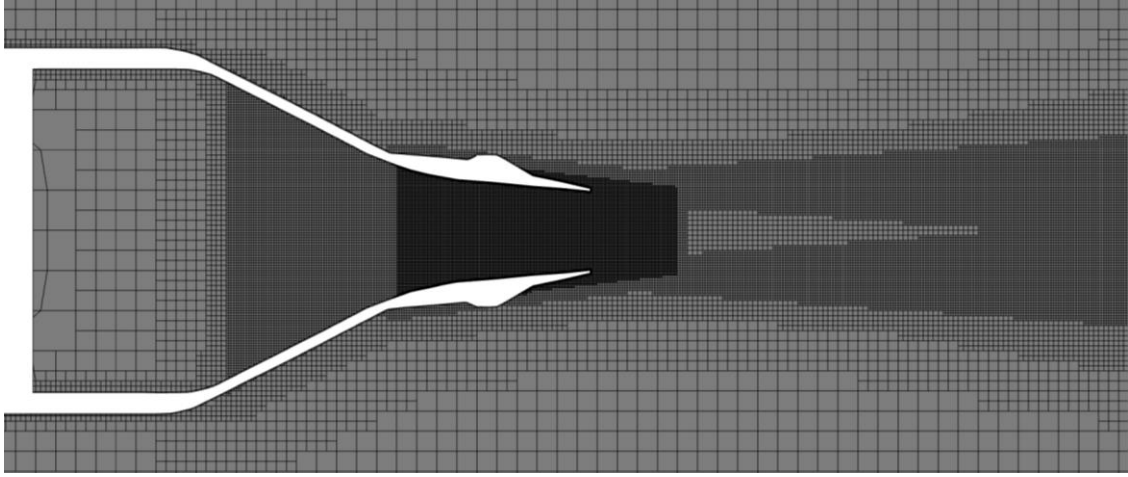


Figure 5: Close up visualization of mesh for SCM000

Due to the no-slip conditions imposed on the nozzle surface and plate and the wall damping effect on the turbulence close to the wall, the boundary layer will have a strong affect on the nozzle flow. The boundary layer has a large gradient normal to the wall with a small gradient tangent to the wall [11], in order to accurately capture the boundary layer interaction with a low Y+ wall treatment, a prism layer mesher is used in order to provide a fine mesh along the surface of the nozzle and plate which aligns with the flow direction. The boundary layer thickness (δ) was estimated using equations 1 and 2 from White F [12], with the values given in Table 1, in order to ensure that a suitable prism layer total thickness is applied to encapsulate the entire boundary layer.

$$Re = \frac{2\rho Vd}{\mu} \quad [1]$$

$$\delta = \frac{0.16d}{Re^{\frac{1}{7}}} \quad [2]$$

Table 1: Boundary layer thickness calculation values

ρ	1.184 kg/m ³
V	169 m/s
d	0.0381 m
μ	1.855x10 ⁻⁵ kg/m-s
Re	8.22x10 ⁵
δ	0.871 mm

From the values calculated in Table 1 a boundary layer total thickness of 1mm was chosen and as the Reynolds number is far greater than 2000 the flow is turbulent, and a turbulent solver will need to be selected[13]. The identified prism layer was applied to the inside surface of the nozzle and lip with a courser prism layer used on outside surfaces with no net flow over the surface to reduce the computational costs. The values are given in Table 2 with the visualisation given in Figure 6 and boundary layer velocity distribution validating the estimation given in appendix , showing an approximate boundary layer thickness of 0.8mm.

Table 2: Prism layer values

Chosen prism layer total thickness (mm)	Number of prism layers	Prism layer stretching
1	15	1.3

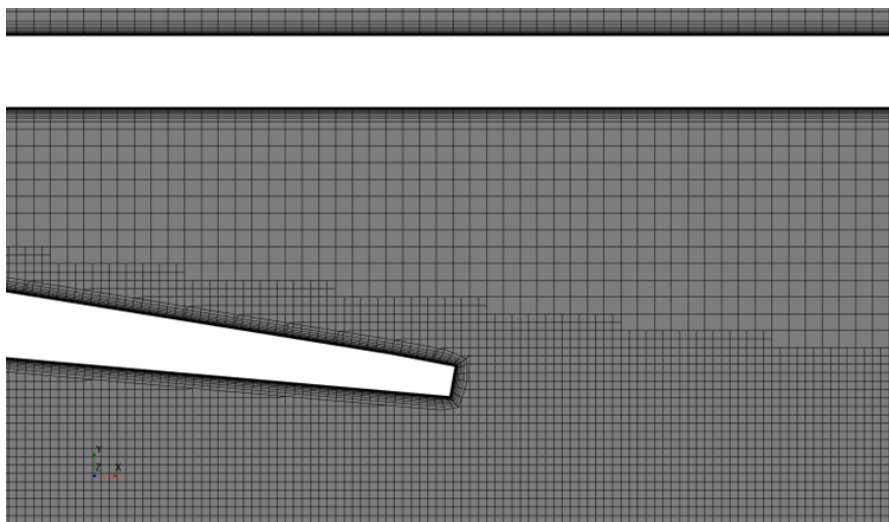


Figure 6: Boundary layer for SMC000

3.3 Boundary Conditions

The 2-dimensional model was setup with a stagnation inlet at the vertical internal nozzle surface, no-slip wall on the nozzle surface and a pressure outlet on all other boundary surfaces. For the 3-dimensional model setup, a stagnation inlet was set on the vertical internal nozzle surface, pressure outlets on the upstream, downstream, and side walls of the control volume with a symmetry plane set on the XY plane at the origin as the jet is symmetrical along the Z axis therefore introducing a symmetry plane significantly reduces the computational resources

required. The nozzle wall was set as a no-slip wall along with the plate in the installed configuration. The atmospheric pressure for the pressure outlets was kept at the default reference pressure of 101325 Pa with the inlet stagnation gauge pressure of 16897 Pa and a temperature ratio of 0.95, as set by Jawahar H et al [7], corresponding to a jet Mach number of 0.5.

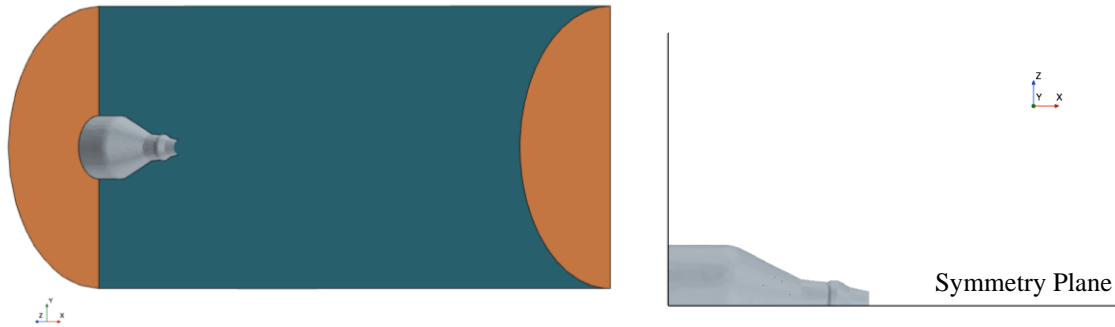


Figure 7: SMC000 boundary conditions

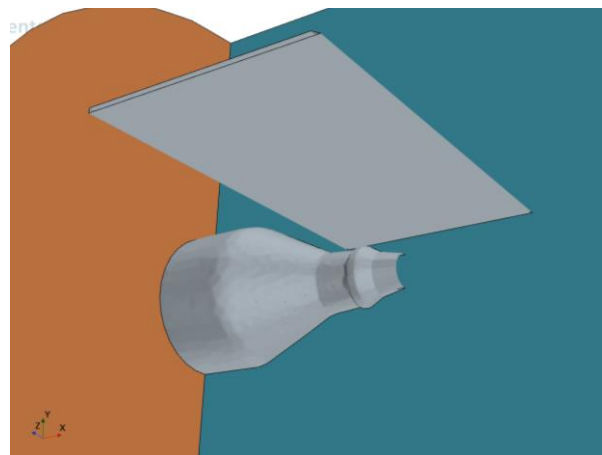


Figure 8: Installed SMC000 boundary conditions

3.4 Data Collection

In order to extract the data required for the numerical analysis a set of probes were set up at various locations depending on the parameters to be sampled. The PlateLine probe measuring the Proudman Acoustic Power spans the surface of the plate along the XY plane from the origin to the end of the plate, a distance of $4D_j$. The LipLine and CentreLine probes measuring the velocity variation with distance start from the X origin, spanning $20D_j$ downstream with the CentreLine being on the origin and the LipLine along the lip line of the top of the nozzle. Six

probes measuring the vertical variations of velocity magnitude and Turbulent Kinetic Energy along the jet plume are placed at $x/D_j = 1, 3, 5, 7, 10, 15$ and span from $-3D_j$ to $1.5D_j$ vertically.



Figure 9: PlateLine, LipLine and CentreLine probes

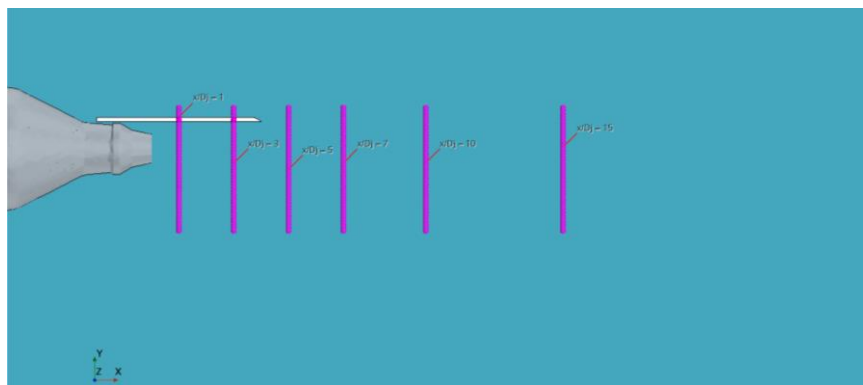


Figure 10: Downstream probes

3.5 Solvers and Models

- Constant Density
 - As the flow Mach number is well below supersonic conditions the compressibility effects can be assumed to be negligible and the constant density solver is suitable with a lower computational requirement.
- Steady
 - The steady model was chosen as it is a more robust solver and significantly more efficient than the unsteady solver. Analysis of the velocity profiles showed a converged steady state solution suggesting the steady state solver is suitable.
- Three Dimensional
 - The three-dimensional solver was selected over the axisymmetric solver for the three-dimensional models as while providing lower computational cost, the

axisymmetric solver assumes a uniform flow over the symmetrical axis which is not suitable.

- Two Dimensional
 - Used for the two-dimensional scenario.
- Segregated Flow with Temperature
 - The flow is subsonic so the segregated solver will provide accurate results at a lower cost.
- Reynolds-Averaged Navier-Stokes
- Turbulent – k-ε
- Broadband Noise – Proudman

4 Results

4.1 Mesh Independence Study

A mesh independence study was carried out in order to ensure that the results obtained were not specific to the mesh used which would show that the results are unreliable. A coarse base size was approximated and then refined until the subsequent results were of a satisfactory deviation. The maximum velocity magnitude at the x/D_j probe was chosen as the monitored variable as it was sufficiently downstream of the nozzle to ensure that disturbances in the flow had been fully resolved. Both the two dimensional and three-dimensional test cases showed adequate mesh independence while aiming to maintain a Y^+ value below 5 in order to accurately capture the boundary layer.

Table 3: 2D mesh independence values. Chosen value highlighted

Number of cells ($\times 10^4$)	Velocity (m/s)	Percentage difference (%)
2.195	170	2.9
4.491	165	12
5.567	145	4.8
7.604	138	2.5
14.49	134.5	0.37
41.54	134	

Table 4: 3D mesh independence values. Chosen value highlighted

Number of cells ($\times 10^5$)	Velocity (m/s)	Percentage difference (%)
2.870	73.4	4.6
3.985	70.0	4.1
7.956	67.1	3.5
12.62	69.5	2.4
25.78	67.8	1.9
37.07	66.5	

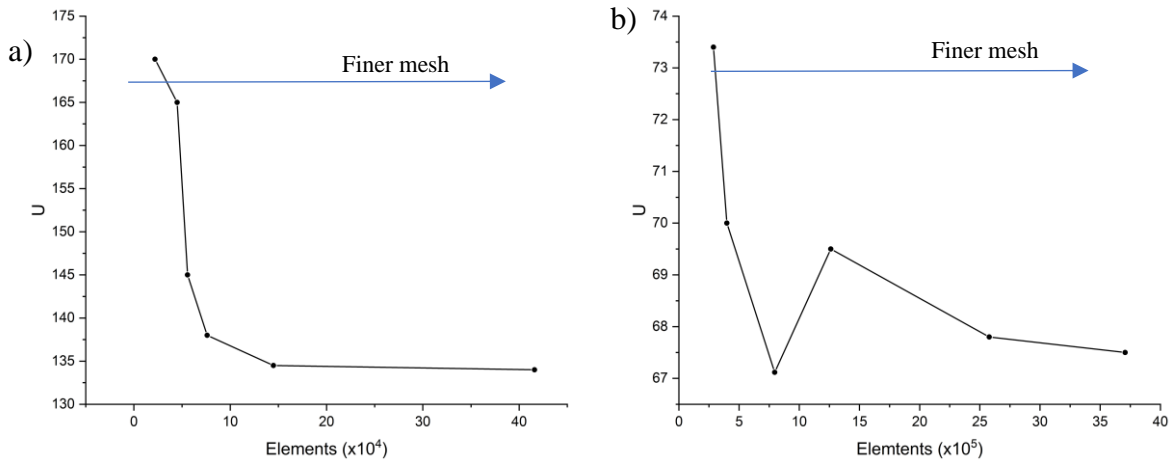


Figure 11: a) 2D, b) 3D mesh independence

The mesh independence study showed that the area of greatest importance was in the nozzle contraction which had the largest velocity gradient in the free flow as well as the boundary layer. An absolute size of 1mm within this section produced a consistently converged result almost independently of the base size, a value larger than 1mm was deemed to produce inaccurate results. This meant that the small area refinement in the nozzle allowed for a coarser overall mesh while producing accurate results, reducing the computational time for converged results. This also showed that the boundary layer thickness estimate was accurate, and the prism layers values given in Table 2 were able to resolve the boundary layer. The chosen mesh refinement is highlighted within Table 3 and 4 and the Y^+ values can be seen in Figure 12.

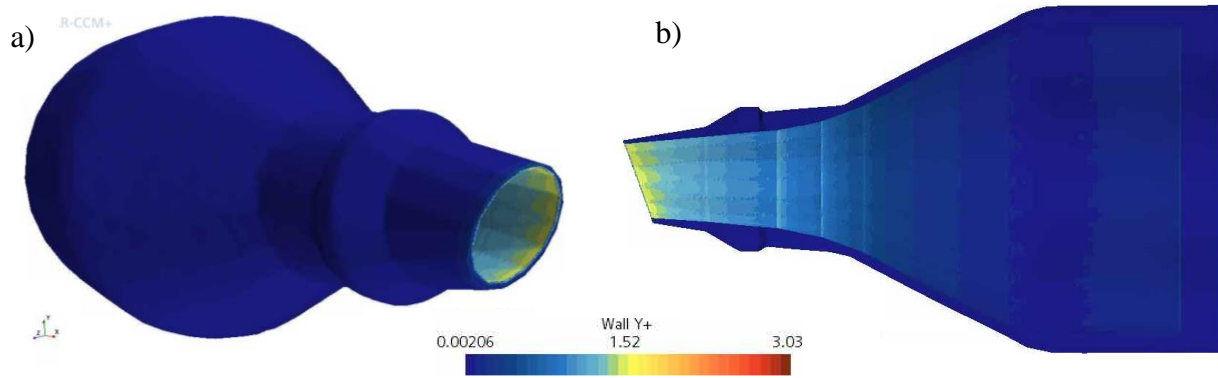


Figure 12: Wall Y^+ distribution on a) external and b) internal nozzle surface

4.2 Preliminary Validation

A preliminary validation was carried out against the RANS isolated SMC000 model by Lyu B et al [8]. The results showed that the three-dimensional solver within STARCCM+ was able to produce comparable results and reliably capture the plume dissipation expected, however the two-dimensional model was unable to produce similar results. This is expected to be due to the two-dimensional solver being unable to calculate the jet plume dissipation in the Z axis as the plume spanned significantly further downstream than is to be expected, therefore the two-dimensional models will not be further implemented. The results by Lyu also show that the results obtained through a RANS model are expected to be lower than that of a LES or experimental study. Figure 14b also shows that there is a marginal difference between installed and isolated scenarios suggesting some jet plume-plate interaction may be occurring.

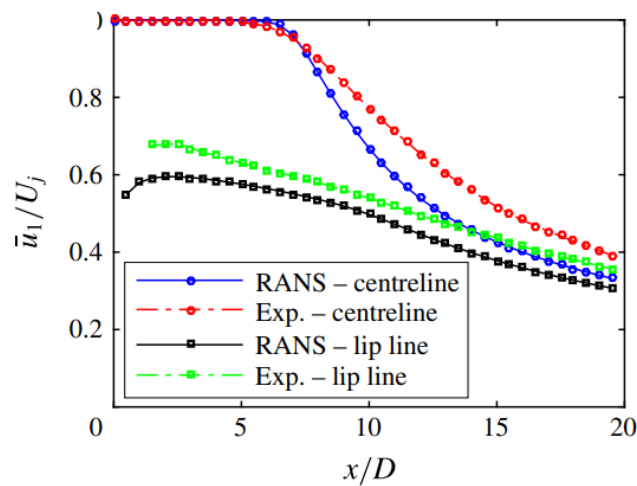


Figure 13: RANS vs LES velocity variation with axial distance [8]

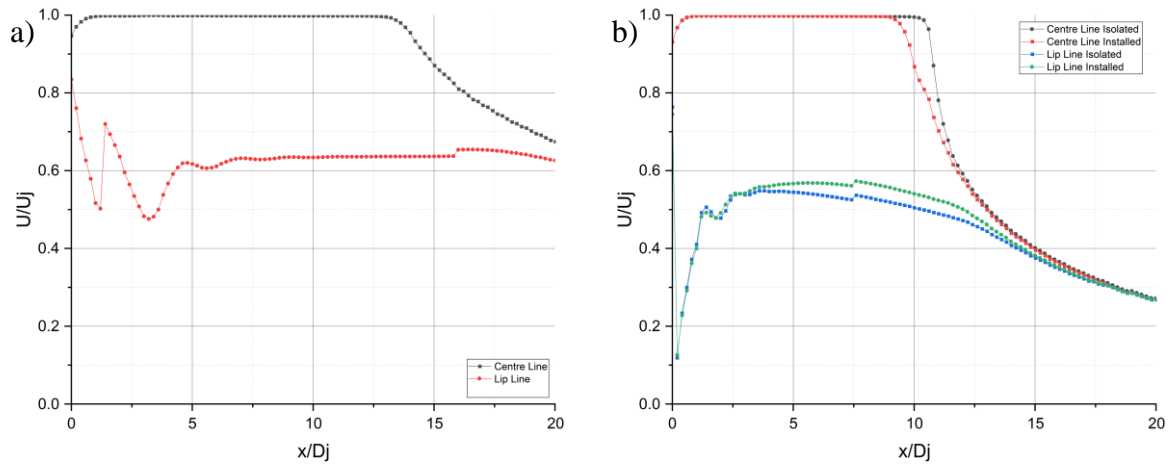


Figure 14: a) 2D Lip and Centre Line plots, b) 3D Lip and Centre line plots installed vs isolated

4.3 Result Convergence

To determine that the simulation had converged to a final steady state value several factors including scalar scene, maximum velocity magnitude plot and residuals. Once fluctuations in the scalar scene were visually observed, residuals were steady and the velocity magnitude was stable within three decimal places over at least 10 iterations, then the simulation can assume to be converged as shown in Figure 15.

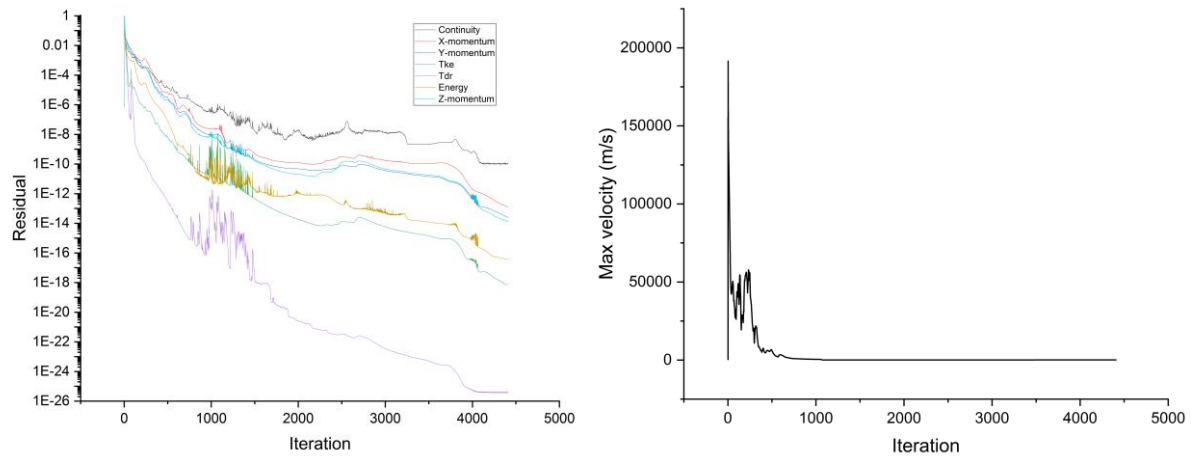


Figure 15: Sample Residual and velocity magnitude plots showing convergence

4.4 Experimental Validation

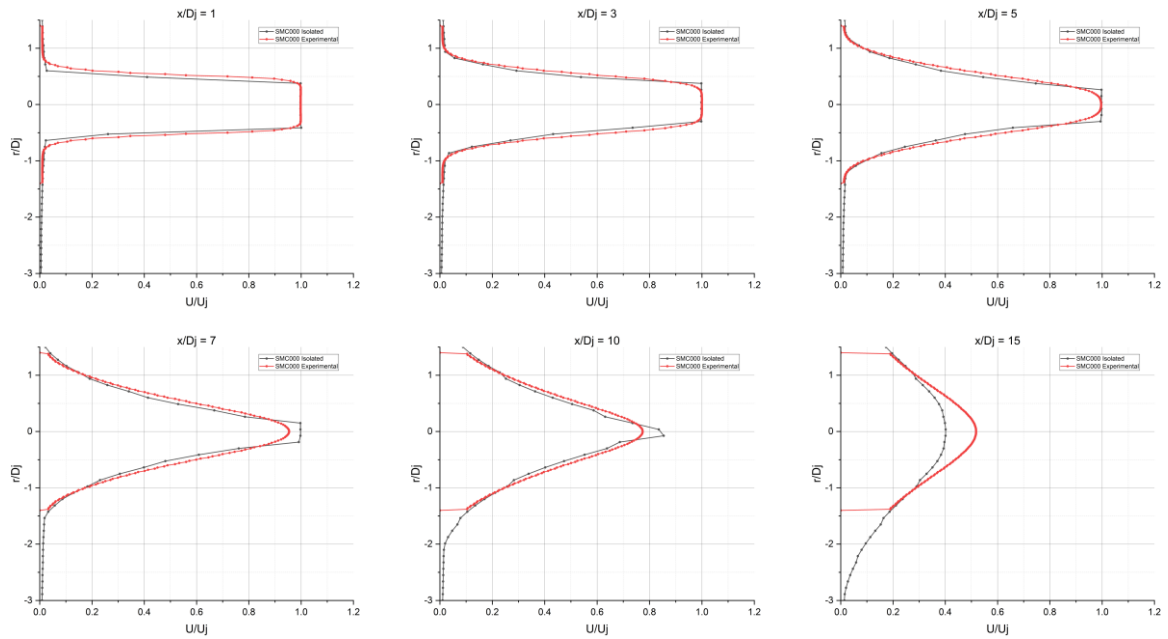


Figure 16: Experimental vs Numerical data for SMC000 nozzle

Table 5: Peak to peak difference

x/D_j	Experimental-Numerical peak-to-peak difference (%)
1	0
3	0
5	0.14
7	4.32
10	7.34
15	22.40

Figure 16 shows the overall agreement of results obtained through the RANS modelling set out in section 3, with the jet plume characteristics being closely matched. The peak-to-peak magnitude difference is shown in Table 5 and it can be seen that the model is accurate up to $x/D_j = 10$ with an approximate error of 7.34% which is acceptable given the low computational costs. Further downstream of the nozzle the error significantly increases however the area of interest within this report is the near field jet characteristics as this is where any jet noise amplification from an installed scenario will happen, therefore accuracy to a x/D_j of 10 is adequate for this investigation. Muller [11] states that the artificial viscosity scales with h^2 for a 2nd order method and that it is most significant in areas with large jumps in cell size, therefore this deviation downstream could suggest that the mesh size increases too quickly inducing a

large artificial viscosity and causing a rapid decrease in velocity. As a thorough mesh independence study was conducted this is unlikely as the study investigated several uniform and non-uniform meshes which converged to the same result, indicating that the far field error is likely due to the steady state assumption.

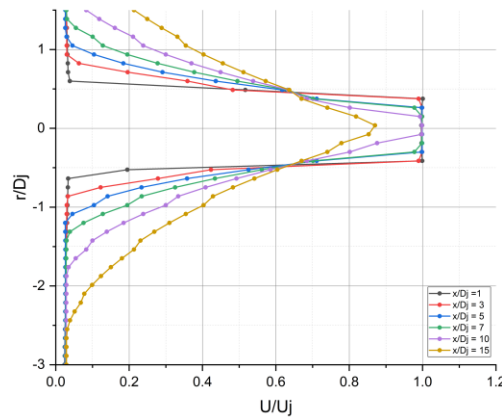


Figure 17: Two-Dimensional SMC000 standardized velocity with radial distance for $x/D_j = 1, 3, 5, 7, 10, 15$

As the two-dimensional model could not be validated and was assumed to be unable to resolve the jet plume for any scenario, any further two-dimensional modelling was halted. Further analysis of the two-dimensional SMC000 isolated model is shown in Figure 17

4.5 Scarfed Nozzle Jet Deflection

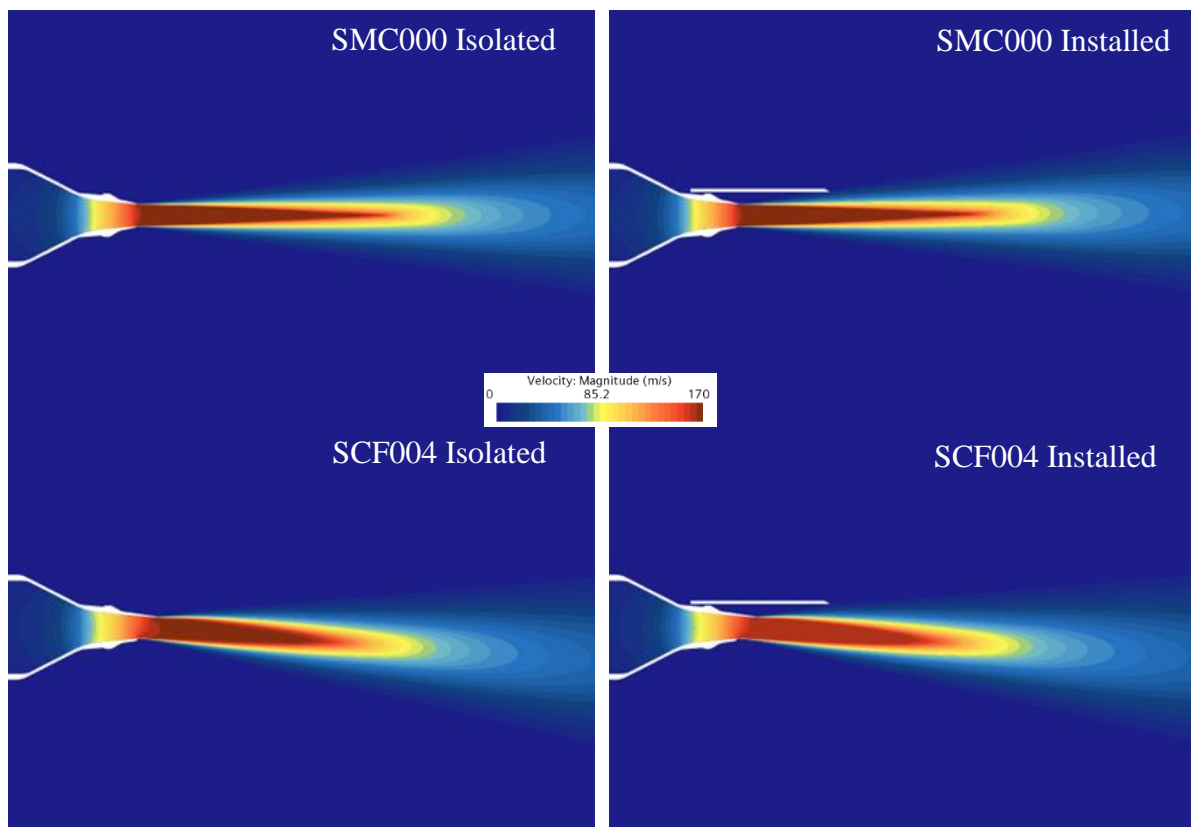


Figure 18: SMC000 and SCF004 jet plume deflection in installed and isolated scenarios

Figure 18 shows the jet plume represented as velocity magnitude for the SMC000 and SCF004 nozzles as both isolated and installed, SCF001-003 can be found in appendix 2. The characteristic deflection between nozzles is noticeable with the SCF004 nozzle providing significant vectoring of the jet, the comparison between isolated and installed configurations shows that the installed configuration deflects the plume slightly towards the plate. A quantitative representation of the jet deflection can be seen in Figures 19-20 and Table 6 showing a uniform and substantial increase in jet deflection of an average of 1.04° per 10° of scarfing angle for an isolated jet and 1.07° per 10° in an installed configuration. The smallest gain in deflection angle is between the SCF002 and 003 nozzles meaning that the weight to performance of the SCF003 is lowest and the largest deflection angle increase comes from the SCF004 nozzle, potentially suggesting an exponential increase in deflection angle with scarf angle however more scarf angles would need to be investigated to conclude this. In addition to the jet deflection, between the SMC000 and SCF004 nozzles a maximum reduction in velocity magnitude of 10% is evident meaning the scarfed nozzles also provide a faster jet plume dissipation suggesting less turbulent noise may be propagated in the far field axial direction[5].

Table 6: Jet deflection angles

Nozzle	Jet deflection angle ($^\circ$) (Isolated)	Jet deflection angle ($^\circ$) (Installed)
SMC000	-0	+0.57
SCF001	-1.15	-0.72
SCF002	-2.43	-2.00
SCF003	-2.86	-2.44
SCF004	-4.15	-3.72

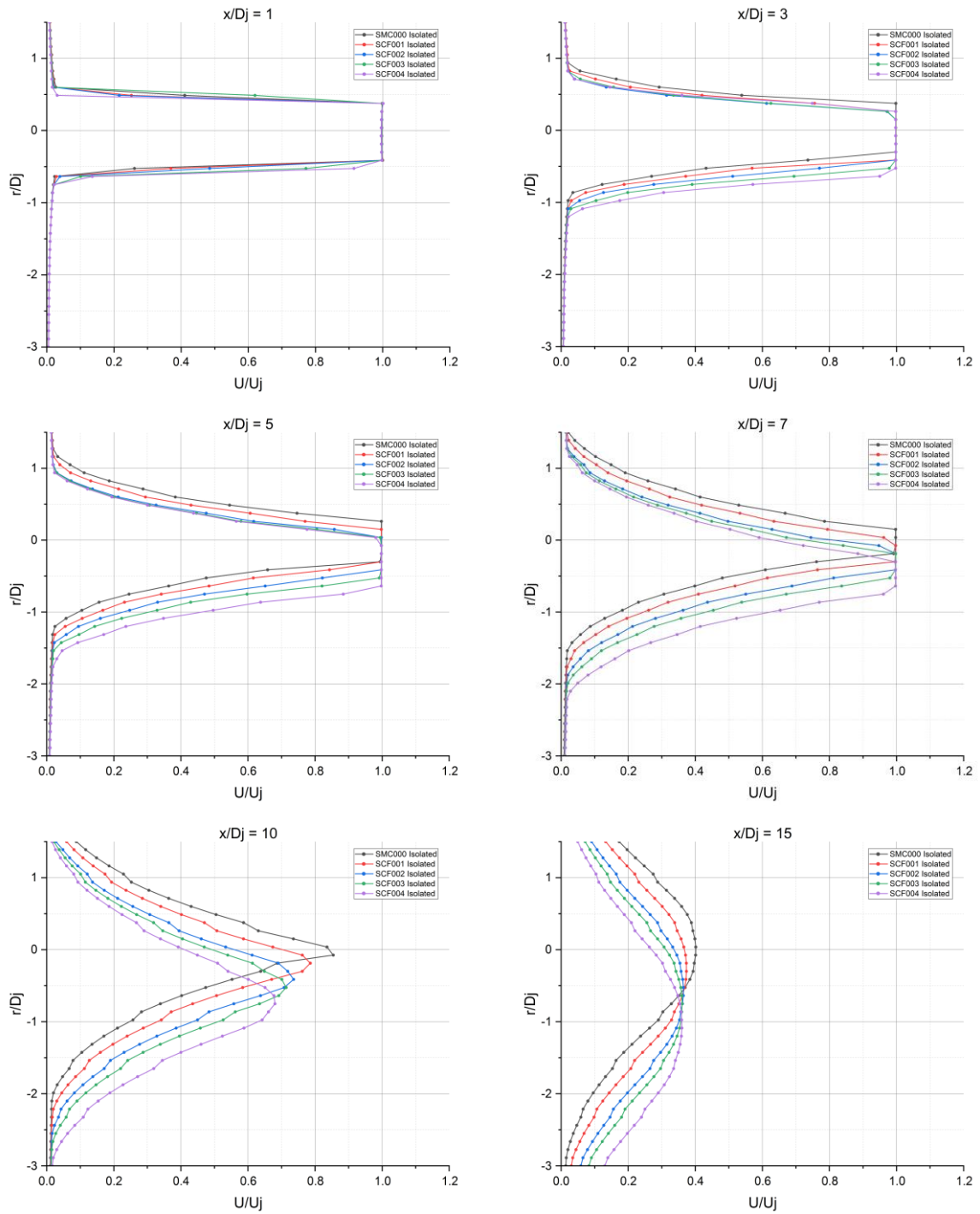


Figure 19: Radial standardized velocity variation for $x/D_j = 1, 3, 5, 7, 10, 15$ (Isolated)

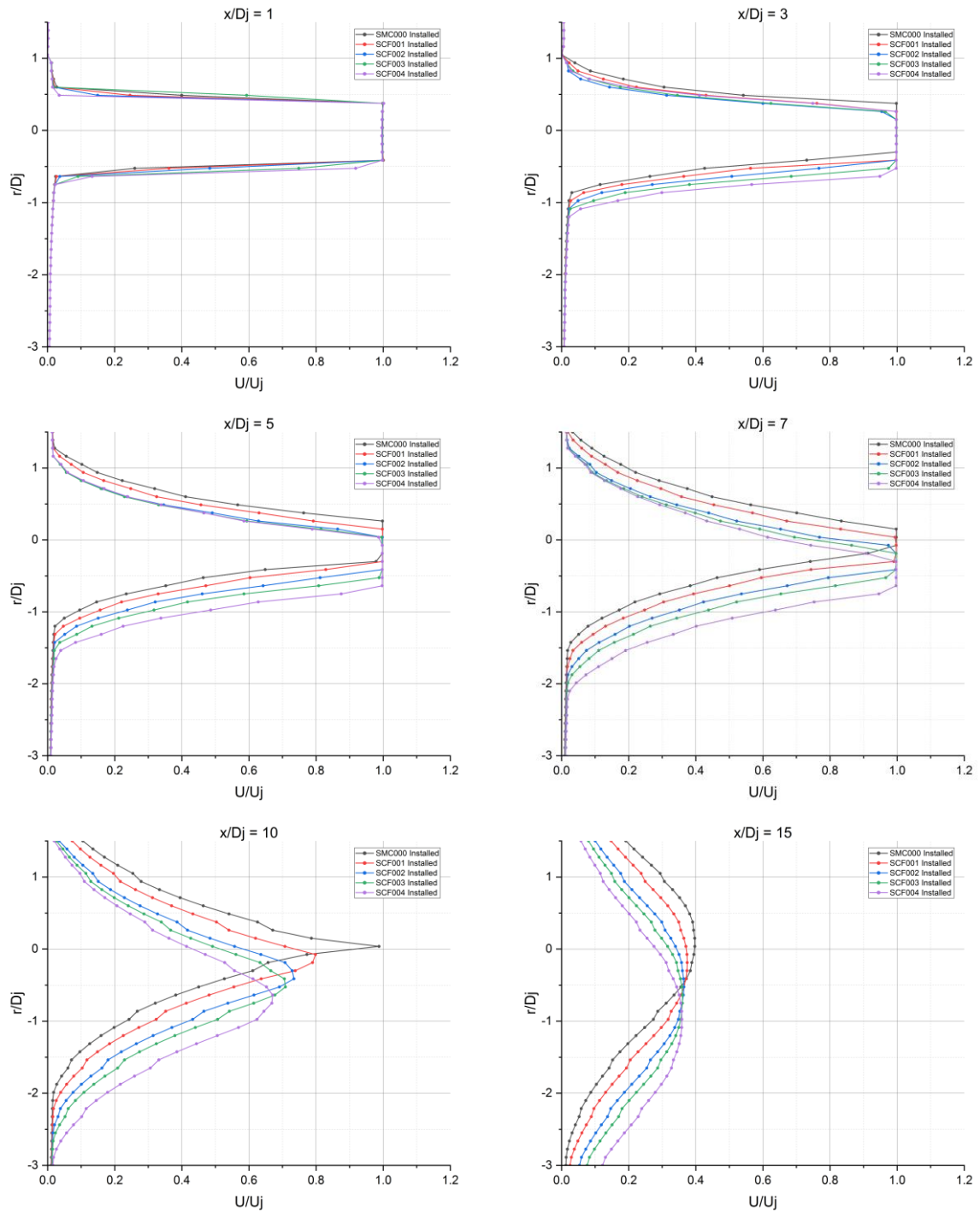


Figure 20: Radial standardized velocity variation for $x/D_j = 1, 3, 5, 7, 10, 15$ (Installed)

4.6 Turbulent Kinetic Energy

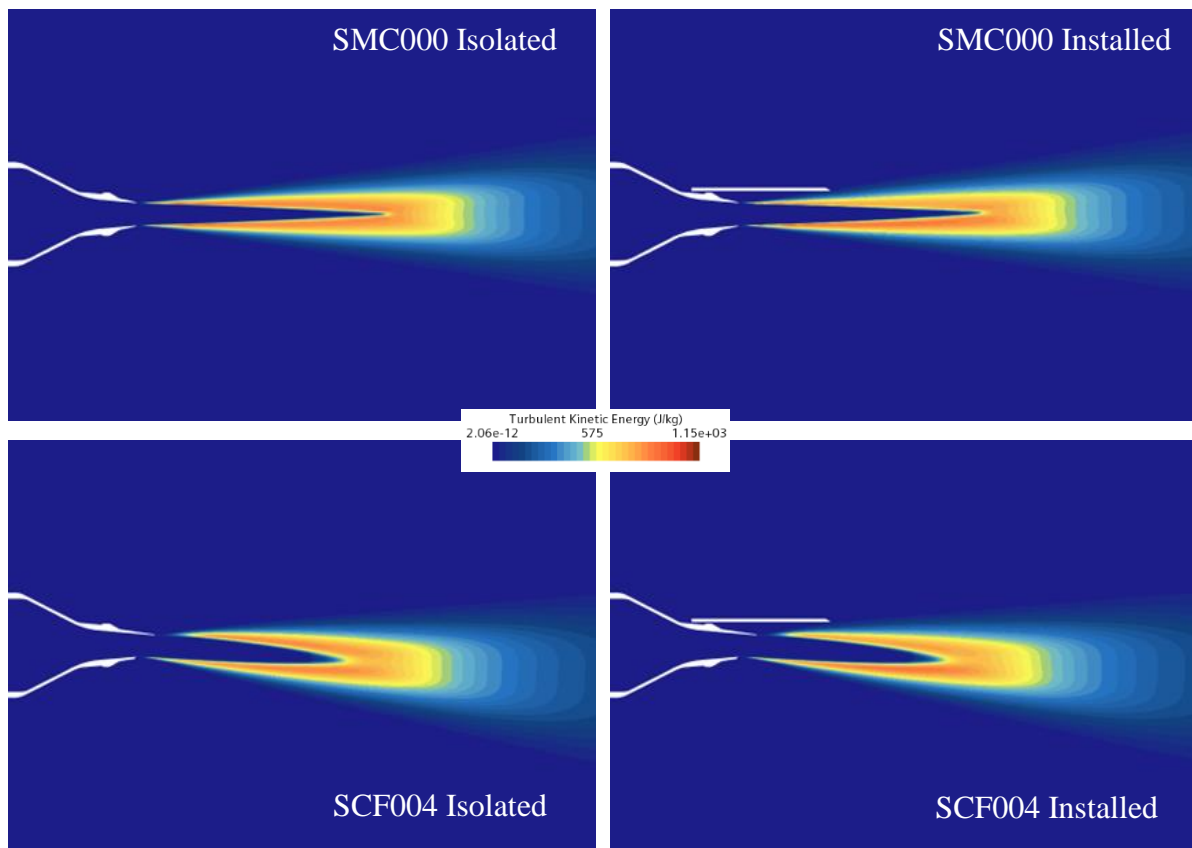


Figure 21: Turbulent Kinetic Energy on XY plane for SMC000 and SCF004 nozzles in isolated and installed scenarios

The turbulent kinetic energy was monitored alongside the velocity magnitude to find any interaction which may be occurring in an installed scenario. Figure 21 shows the turbulent kinetic energy is deflected with the plume along the XY axis, where it is most visible between the SMC000 and SCF004 nozzles and SCF001-003 can be found in appendix 3, the turbulence is also shown to dissipate faster with a scarfed nozzle. The installed cases for all nozzles show a decrease in turbulent energy along the top lip line as compared to their isolated counterpart with a higher scarf angle showing a smaller decrease in said turbulence, shown in Figure 22. As supported by Launder, turbulent flow experiences damping of the turbulent energy when in close proximity to a surface [14], this decrease in turbulent energy along the top lip line coincides with the jet deflection towards the plate in section 4.5 proving that at a plate distance of $1D_j$ there is interaction between the jet turbulent flow and plate.

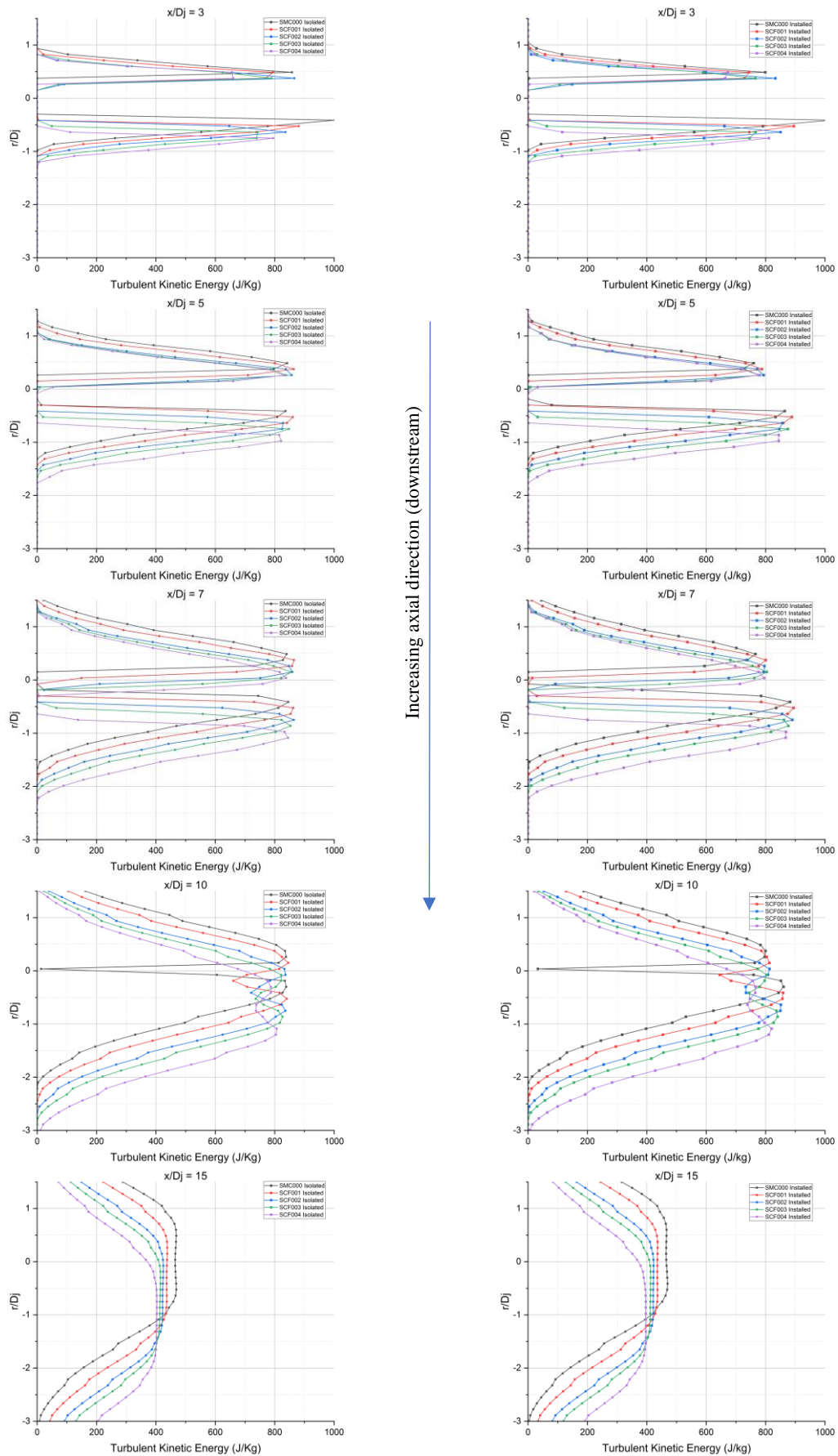


Figure 22: The variation in the radial direction at $x/D_j = 3, 5, 7, 10, 15$ for all nozzles in isolated vs installed scenarios

4.7 Acoustics

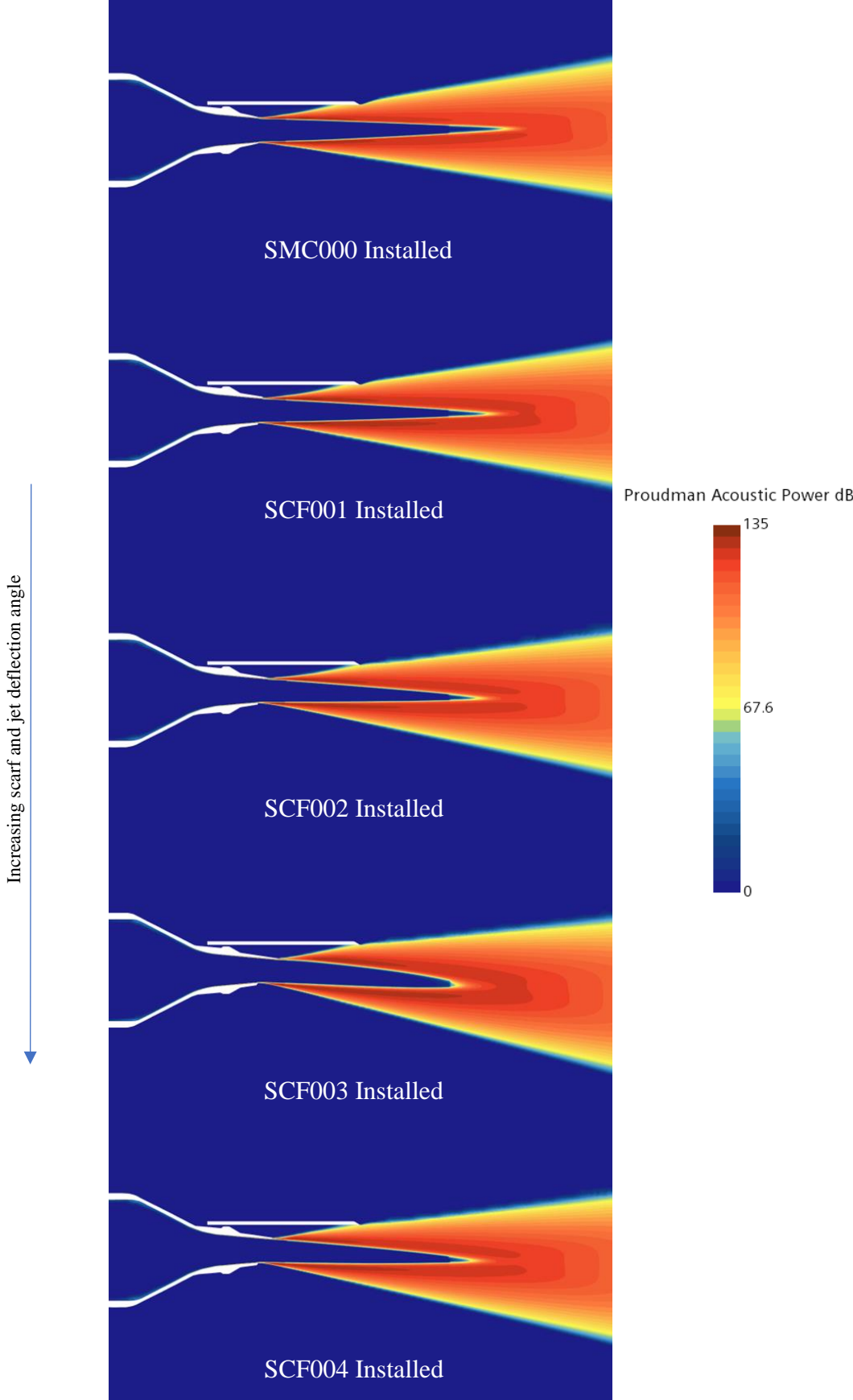


Figure 23: Proudman Acoustic Power for all installed nozzles on XY plane

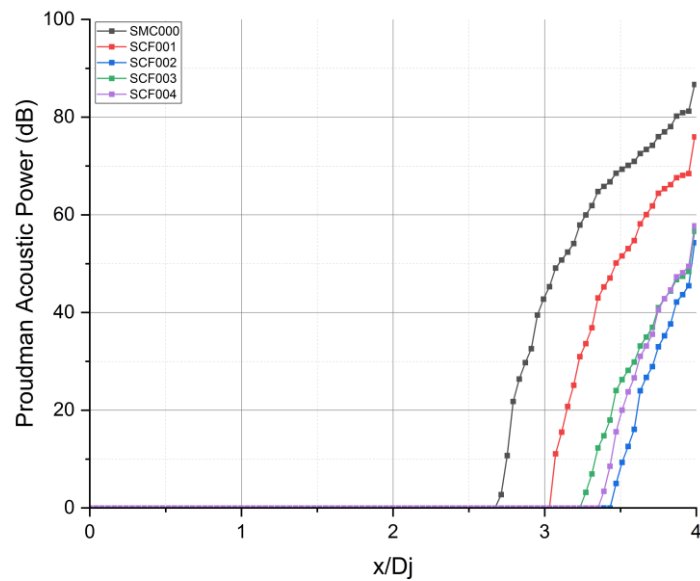


Figure 24: Proudman acoustic power along the lower plate surface for installed nozzles

In a RANS model the nearfield contribution towards acoustic power can be represented using the Proudman broadband noise source model which evaluates the noise contribution due to a turbulent flow [15]. Due to the constrictions of this report a far field noise or sound pressure level model could not be formulated however, the near field Proudman model can be used to characterise the effects of a plate on the noise output of an installed nozzle. As previously mentioned, the noise amplification from a plate surface is due to two phenomenon which occur on the plate, those being surface scrubbing and edge scattering[3]. Figure 23 shows the Proudman acoustic power on the XY plane and it can be seen that the acoustic power is deflected away from the plate by the scarfed nozzles, following the jet plume. For the SMC000 nozzle the plate has a large interaction with the acoustic power source leading to a non-uniform field whereas the effect of the scarf angles on the SCF nozzles almost completely eliminate this interaction. Figure 24 further supports the reduced interaction as both the surface span at which interaction occurs and the magnitude of the acoustic power on the plate trailing edge is significantly reduced with scarf angle. The Proudman acoustic model shows a potential significant reduction in installed noise when comparing the scarfed nozzles to a round symmetrical nozzle, with the SCF004 nozzle a reduction of 52.1% in surface interaction and 34.7% reduction in acoustic power at the scattering edge was seen meaning that the scrubbing and scattering effects established by brown would also see a significant reduction. This is in agreement with Brown's findings [3], the installation noise being proportional to the plate-centreline radial distance, as the scarfed nozzles deflect the jet centreline away from the plate.

In table 7 the reductions from the SCF002 nozzle are disproportionate suggesting the SCF002 nozzle is a likely outlier.

Table 7: Plate interaction reduction for installed scarfed nozzles

Nozzle	Surface span reduction (%)	Edge acoustic power magnitude reduction (%)
SCF001	27.1	12.4
SCF002	57.1	37.3
SCF003	42.1	33.3
SCF004	52.1	34.7

4.8 Computational Expenses

The project set out to find a computationally efficient analysis of nozzles within the investigation, the Apocrita HPC was utilised running simulations on 16 cores with an average turn around under two hours, as shown in Table 8, which is substantially lower than a LES or experimental setup while providing adequate results.

Table 8: Computational resources used

Number of CPU cores	16
Max rss (RAM usage) (Gb)	8.5
Average Isolated hrt (hours)	~ 1.5
Average Installed hrt (hours)	< 2

5 Conclusion

A numerical analysis using the RANS equations was conducted on the round symmetrical SMC000 nozzle and scarfed SCF001-004 nozzles in an isolated and installed configuration to quantify the affects of a surface in a close proximity of $1D_j$ to the nozzle. The analysis was conducted based on the experimental data of Jawahar et al at the University of Bristol where an experimental analysis of these nozzles was conducted. Results were validated against similar theoretical papers as well as experimental data provided for the purpose of validation of numerical methods. It was found that a jet deflection of approximately 1° can be achieved per 10° of scarf angle on the nozzle, that a scarfed nozzle provided faster plume dissipation over the SMC000 nozzle and that the presence of a plate near the nozzle caused deflection of the jet

towards the plate. The plate acted as a dampener for turbulent kinetic energy along the top lip line for an installed nozzle which showed interaction between the plate boundary layer and Tke and that a scarfed nozzle reduces this effect. Furthermore, it was concluded that a SCF004 nozzle can produce 52.1% less acoustic plate interaction and 34.7% lower acoustic power magnitude on the plate trailing edge, over the SMC000 nozzle, which would suggest a significant reduction in installed noise. It must be noted that a quantitative noise reduction model in the far field could not be achieved, and the results obtained for the SCF002 nozzle do not follow the general trend of the other scarfed nozzles and is deemed to be an outlier within the scope of this investigation. Further development of the far field noise models is required as well as re-modelling of the SCF002 model.

6 References

- [1] ICAO, *Annex 16*, Eighth Edition., vol. 1. International Civil Aviation Organization, 2017.
- [2] ICAO, “NOVEL AIRCRAFT-NOISE TECHNOLOGY REVIEW AND MEDIUM- AND LONG-TERM NOISE REDUCTION GOALS,” Montreal, 2014.
- [3] C. A. Brown, “Jet-surface interaction test: Far-field noise results,” *J Eng Gas Turbine Power*, vol. 135, no. 7, 2013, doi: 10.1115/1.4023605.
- [4] F. Saeed, “Saeed Farokhi Second Edition Aircraft Propulsion,” 2014.
- [5] H. K. Jawahar, A. P. Markesteijn, S. A. Karabasov, and M. Azarpeyvand, “Effects of Chevrons on Jet-installation Noise,” in *AIAA Aviation and Aeronautics Forum and Exposition, AIAA AVIATION Forum 2021*, American Institute of Aeronautics and Astronautics Inc, AIAA, 2021. doi: 10.2514/6.2021-2184.
- [6] C. J. Mead and J. R. Strange, “Under-Wing Installation effects on Jet Noise at Sideline,” 1998.
- [7] H. K. Jawahar and M. Azarpeyvand, “Scarfed Nozzle for Jet Installation Noise Reduction,” in *28th AIAA/CEAS Aeroacoustics Conference, 2022*, American Institute of Aeronautics and Astronautics Inc, AIAA, 2022. doi: 10.2514/6.2022-2908.
- [8] B. Lyu, A. P. Dowling, and I. Naqavi, “Prediction of installed jet noise,” *J Fluid Mech*, vol. 811, pp. 234–268, Jan. 2017, doi: 10.1017/jfm.2016.747.
- [9] H. A. Abid, A. P. Markesteijn, V. Gryazev, S. A. Karabasov, H. K. Jawahar, and M. Azarpeyvand, “Jet Installation Noise Modelling Informed by GPU LES,” in *28th AIAA/CEAS Aeroacoustics Conference, 2022*, American Institute of Aeronautics and Astronautics Inc, AIAA, 2022. doi: 10.2514/6.2022-2906.
- [10] U. Piomelli, “Large-eddy simulation: achievements and challenges,” 1999.
- [11] J.-D. Muller, *Essentials of computational fluid dynamics*. CRC Press, 2015.
- [12] F. M. White, *Viscous fluid flow*. McGraw-Hill, 1991.
- [13] H. Schlichting and J. Kestin, *Boundary layer theory*, vol. 121. Springer, 1961.
- [14] B. E. Launder and W. Rodi, “THE TURBULENT WALL JET-MEASUREMENTS AND MODELING,” 1983. [Online]. Available: www.annualreviews.org
- [15] S. Sarkar and M. Y. Hussaini, “COMPUTATION OF THE SOUND GENERATED BY ISOTROPIC TURBULENCE,” 1993.

7 Appendix

7.1 Boundary layer analysis

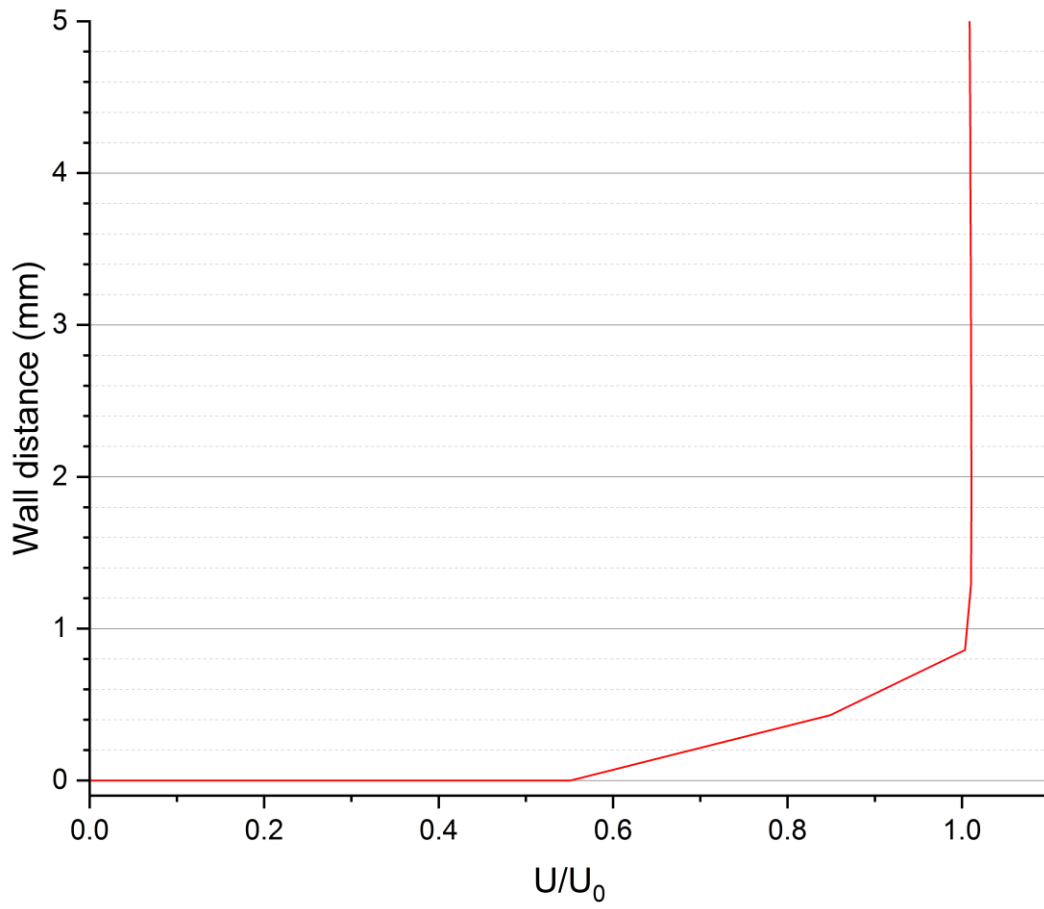


Figure 25: Boundary layer characteristics at nozzle exit

7.2 Velocity scalar scenes for section 4.5

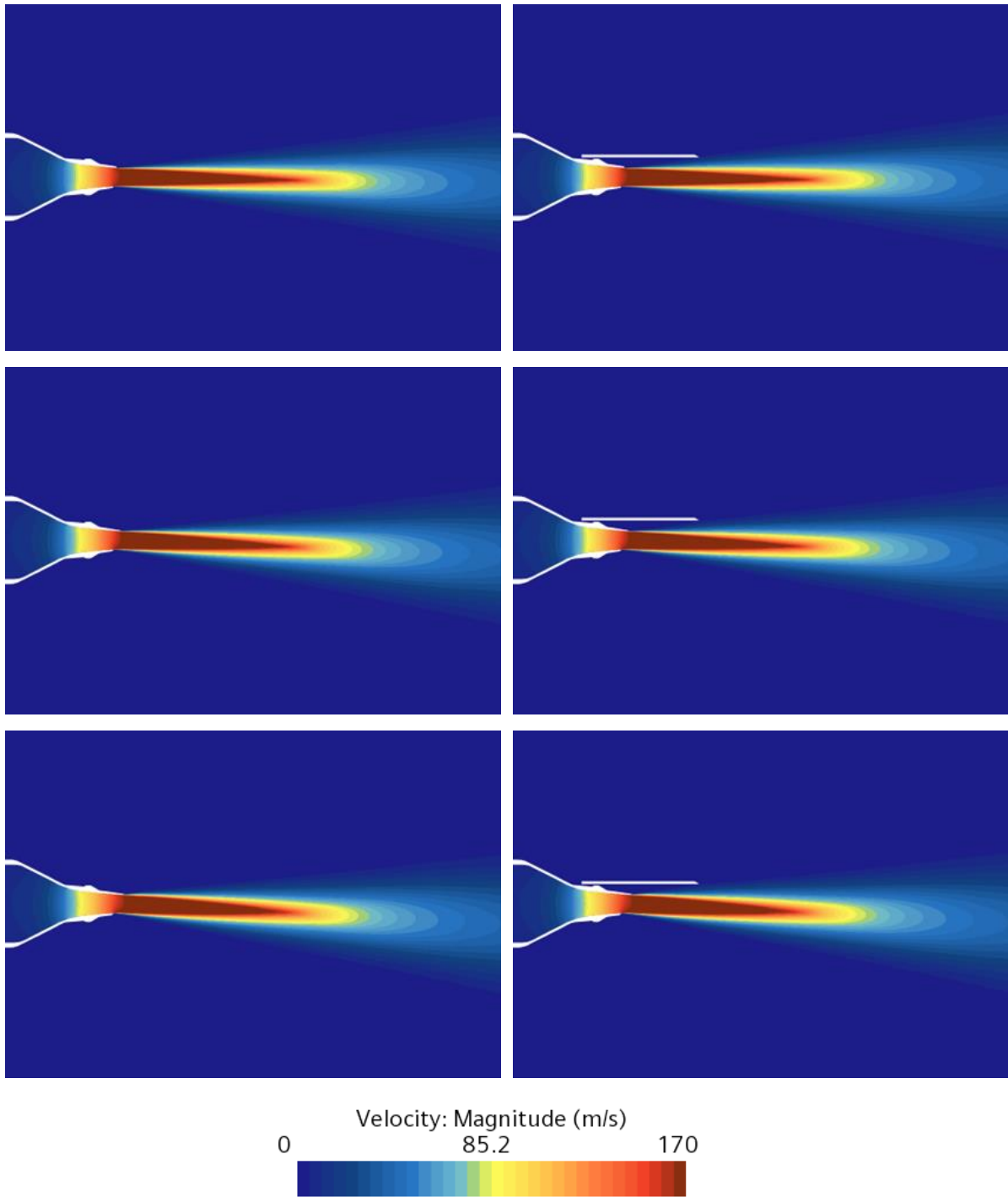


Figure 26: Installed and Isolated velocity scalar scenes for nozzles SCF001-003

7.3 Turbulent kinetic energy scalar scenes for section 4.6

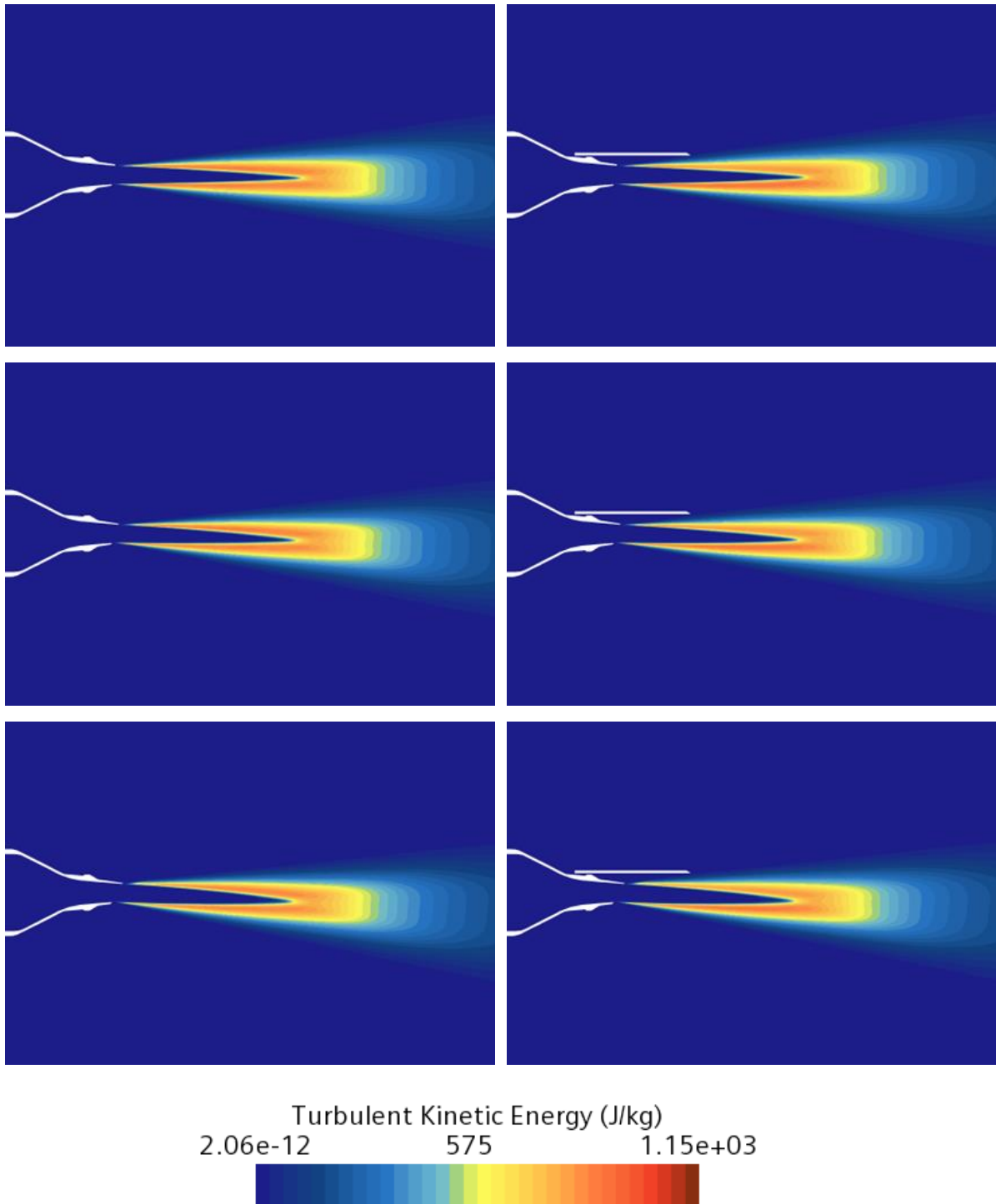


Figure 27: Installed and Isolated turbulent kinetic energy scalar scenes for nozzles SCF001-003